JOC The Journal of Organic Chemistry

Article

pubs.acs.org/joc

Synthesis, Photophysical Properties, and Application of *o*- and *p*-Amino Green Fluorescence Protein Synthetic Chromophores

Yi-Hui Chen, Wei-Jen Lo, and Kuangsen Sung*

Department of Chemistry, National Cheng Kung University, Tainan, Taiwan

Supporting Information

ABSTRACT: The *o*- and *p*-amino green-fluorescence-protein synthetic chromophores (GFPSCs) were synthesized from the corresponding *o*- and *p*-nitro protecting group. Among the four protecting groups of the *o*-amino group, the *o*-nitro protecting group is the only choice to synthesize the *o*-amino GFPSCs. The first singlet excited states of *o*- and *p*-amino GFPSCs carry significant charge-transfer character through the mechanism of photoinduced charge transfer (PCT). The *o*-amino GFPSCs can serve as wavelength-ratiometric fluorescence sensors that selectively recognize Cr^{3+} in aqueous medium through a PCT mechanism.

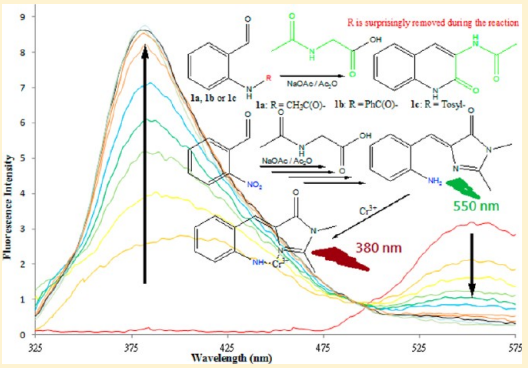

INTRODUCTION

The green fluorescent protein (GFP) and its family have been emerging as powerful probes for intracellular dynamics.[1] The GFP absorbs at 395 nm (neutral form) with a weaker absorption at 475 nm (anion form) and emits green light at 508 nm that is anion emission caused by intermolecular excited-state proton-transfer (ESPT).[1] When the GFP is stripped of the protein environment, the central free chromophore of *p*-hydroxybenzylidenedimethylimidazolone (*p*-HBDI) does not display a tautomer emission through intermolecular ESPT in all solvents,[2b] and its fluorescence quantum yield significantly decreases because of photoisomerization decay or internal conversion.[3] On the other hand, *o*-HBDI shows a tautomer emission at 600 nm that involves excited-state intramolecular proton transfer (ESIPT).[2a,c] We wondered how replacement of the hydroxyl group of GFP chromophore with an amino group might alter its photophysics and what its potential application might be.

Trivalent chromium, Cr^{3+}, is an important trace element in human biological systems because it involves several biochemical processes.[4a,b] Diabetes and cardiovascular diseases are associated with Cr^{3+} deficiency.[4c] Cellular structures can be negatively affected by exposure to high level of Cr^{3+}.[4d] Hence, detection of trace Cr^{3+} is in high demand. Because of its simplicity, high sensitivity, and instantaneous response, fluorescence detection of metal ions usually provides great advantages over other detection techniques. There are some photoluminescent ratiometric[5a,b] or turn-on[5c−i] sensors that were developed for recognition of Cr^{3+} through the following chromophore/mechanism: heavy metal complex/PET,[5a] rodamine/ring-opening (or FRET),[5b,f−h] chalcogeno podand/conformation change,[5c] BODIPY/PET,[5d] dansyl/PET,[5e] and 4-aminophthalimide/PET.[5i] In spite of these advances, the sensors still suffer from some inadequacies like selectivity, reversibility, or use in aqueous medium. In this paper, we used *o*-amino GFPSC as a chromophore and photoinduced charge transfer (PCT) as a sensing mechanism to develop wavelength-ratiometric fluorescence sensors that selectively recognize Cr^{3+} and can be used in aqueous medium.

COMPUTATIONAL DETAILS

All of the calculations reported here were performed with the Gaussian03 program.[6] Geometry optimization of *o*-**4**, *o*-**7**, and *p*-**7** was carried out at B3LYP/6-31+G* without any symmetry restriction. After the geometry optimization was performed, analytical vibration frequencies were calculated at the same level to determine the nature of the located stationary point. Time-dependent density functional theory (TDDFT) was used to calculate the vertical electronic transitions of the first 5 states of *o*-**4**, *o*-**7**, and *p*-**7** in the gas phase and the electron-density surfaces of their molecular orbital at the level of B3LYP-TD/cc-PVDZ//B3LYP/6-31+G*.

RESULTS AND DISCUSSION

Synthesis. One of the potential problems for the preparation of *o*-**4** is that the *o*-amino group as a good nucleophile may undergo intramolecular cyclization during syntheses. To solve the problem, our strategy is to use four kinds of protecting groups for the *o*-amino group, and its retrosynthesis is outlined in Scheme 1.

Because 5-oxazolone is susceptible to nucleophilic attack,[7] we recovered the *o*-amino group after the 5-oxazolone was converted to 5-imidazolone. In this retro-synthesis, *o*-**2a** was

Received: September 27, 2012
Published: November 29, 2012

Scheme 1. Retro-synthesis of *o*-Amino GFPSC (*o*-4)

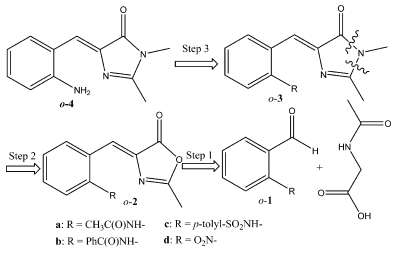

been obtained by Gucky via step 1.[8] However, we attempted this reaction many times with various conditions, and we always obtained **5** instead of *o*-**2a** (Scheme 2). The *o*-acetamido group undergoes intramolecular cyclization and fails to serve as a protecting group of the *o*-amino group.

Scheme 2. Reaction of *o*-1a with NaOAc/Ac_2O in the Presence of *N*-Acetylglycine under Reflux

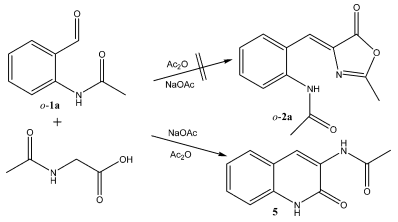

When *o*-**1a** reacted with NaOAc/Ac_2O under reflux in the absence of *N*-acetylglycine, **6** was generated and the *o*-amido group also became involved in the intramolecular cyclization, indicating that α-carbanion of the *o*-acetamido group serves as a nucleophile for the cyclization reaction (Scheme 3). Thus, we

Scheme 3. Reaction of *o*-1a with NaOAc/Ac_2O in the Absence of *N*-Acetylglycine under Reflux

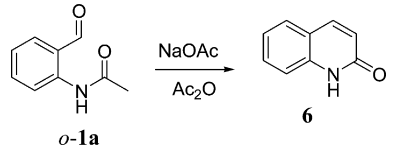

used the *o*-benzamido group to replace the *o*-acetamido group as a protecting group of the *o*-amino group. Then, *o*-**1b** reacted with NaOAc/Ac_2O under reflux in the presence of *N*-acetylglycine, and **5** was generated again (Scheme 4). The *o*-benzamido group also became involved in the intramolecular cyclization. The strange thing is that the benzoyl group was removed during the reaction. Hence, we replaced the *o*-benzamido group with *o*-tosylamido group as a protecting

Scheme 4. Reaction of *o*-1a, *o*-1b or *o*-1c with NaOAc/Ac_2O in the Presence of *N*-Acetylglycine under Reflux

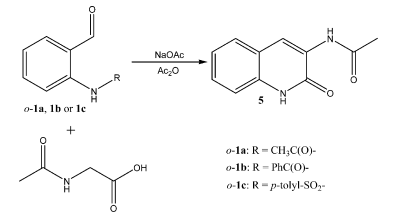

group of the *o*-amino group. When *o*-**1c** reacted with NaOAc/Ac_2O under reflux in the presence of *N*-acetylglycine, **5** was generated again and the tosyl group was also removed during the intramolecular cyclization. It is unusual that the acety, benzoyl, and tosyl groups are removed from the *o*-amino group during the intramolecular cyclization.

Because *o*-acetamido, *o*-benzamido, and *o*-tosylamido groups fail to serve as protecting groups for the *o*-amino group in the preparation of *o*-**4**, we used the nitro group as a protecting group of the *o*-amino group. When *o*-**1d** reacted with NaOAc/Ac_2O under reflux in the presence of *N*-acetylglycine, *o*-**2d** was generated and no intramolecular cyclization occurred (Scheme 5). To convert 5-oxazolone to 5-imidazolone, *o*-**2d** was treated

Scheme 5. Synthesis of *o*- and *p*-Amino GFPSCs

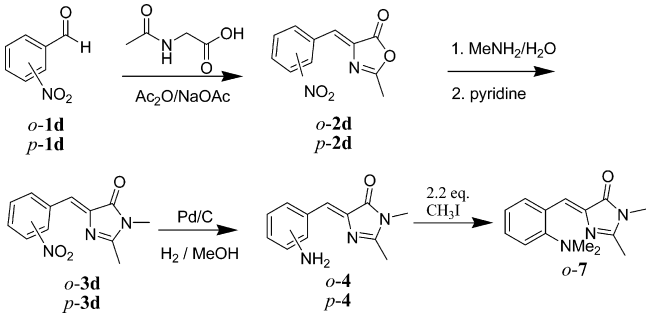

with methylamine, followed by reflux in pyridine, to obtain *o*-**3d**, and then the *o*-amino group was recovered by Pd-catalyzed hydrogenation of *o*-**3d** in MeOH. We tried to use $SnCl_2$ or Fe to reduce the NO_2 group of *o*-**3d**, but these reactions led to very complicated products. The *o*-*N*,*N*-dimethylamino analogue *o*-**7** was produced by treating *o*-**4** with 2.2 equiv of methyl iodide.

Photophysics. The lowest energy electronic absorption bands of *o*-**4**, *o*-**7**, *p*-**4**, and *p*-**7** in acetonitrile are located at 422 ($\varepsilon = 5.3 \times 10^3$ M^{-1} cm^{-1}), 396 ($\varepsilon = 6.7 \times 10^3$ M^{-1} cm^{-1}), 394 ($\varepsilon = 2.7 \times 10^4$ M^{-1} cm^{-1}) and 422 ($\varepsilon = 2.5 \times 10^4$ M^{-1} cm^{-1}) nm, respectively (Table 1). To understand whether the lowest

Table 1. Photophysical Properties of *o*- and *p*-Amino GFPSCs at Room Temperature

	o-4		*o*-7		*p*-7	
solvent	abs[a]	em[a]	abs[a]	em[a]	abs[a]	em[a]
C_6H_{12}	427	451, 465 (2)	395	472 (10)	405	437 (0.1)
CH_2Cl_2	422	452, 489 (4)	396	535 (6)	428	482 (0.9)
THF	430	513 (9)	395	519 (14)	419	452 (0.4)
CH_3CN	422	453, 524 (4)	396	536 (8)	422	483 (0.3)
DMSO	436	530 (7)	398	552 (5)	434	490 (0.2)
CH_3OH	424	454, 520 (2)	398	522 (3)	435	492 (0.3)
H_2O	390	452, 488 (1)	346	426 (3)	446	520 (0.2)

[a]Unit: nm; emission wavelength with fluorescence quantum yield ($\phi_f \times 10^{-3}$) in parentheses.

energy electronic absorption band of *o*-**4**, *o*-**7**, *p*-**4**, and *p*-**7** involves a charge-transfer absorption, we use nitrobenzene as a reference and do calculations on its charge-transfer absorption by TDDFT. It is known that an observed charge-transfer absorption of nitrobenzene is located at 252 nm with $f = 0.17$.[9] Its calculated charge-transfer absorption, which is contributed by 0.64[HOMO-1→LUMO]-0.13[HOMO→LUMO+1], with

dx.doi.org/10.1021/jo302050y | J. Org. Chem. 2013, 78, 301−310

Table 2. Calculated and Observed Electronic Absorption, Oscillator Strength (f), and Transition Electric Dipole Moment (μ_{tr}) of Nitrobenzene, *o*-4, *o*-7, and *p*-7

	λ_{abs}(nm)		f		μ_{tr} (au)		
compd	calcd/level[a]	exptl	calcd	exptl	x	y	z
nitrobenzene	255[b]/A	252[f]	0.1963	0.17[f]	1.2837	0	0
nitrobenzene	249[b]/B	252[f]	0.1902	0.17[f]	1.248	0	0
o-**4**	415[c]/B	427[g]	0.2894	0.11[g]	−1.9	−0.59	0
o-7	410[d]/B	395[g]	0.2153	0.17[g]	1.7	0.05	−0.08
p-7	382[e]/B	405[g]	0.9418	0.52[g]	−3.4	0.11	0

[a]A: B3LYP-TD/cc-PVTZ//B3LYP/6-31+G*. B: B3LYP-TD/cc-PVDZ//B3LYP/6-31+G*. [b]This is the charge-transfer absorption[9] contributed by 0.64[HOMO-1→LUMO] −0.13[HOMO→LUMO+1]. [c]This is the lowest energy electronic absorption contributed by 0.61[HOMO→ LUMO]-0.18[HOMO-1→LUMO]. [d]This is the lowest energy electronic absorption contributed by 0.58[HOMO→ LUMO]-0.33[HOMO-1→LUMO]. [e]This is the lowest energy electronic absorption contributed by 0.61[HOMO→ LUMO]. [f]Reference 9. [g]In cyclohexane.

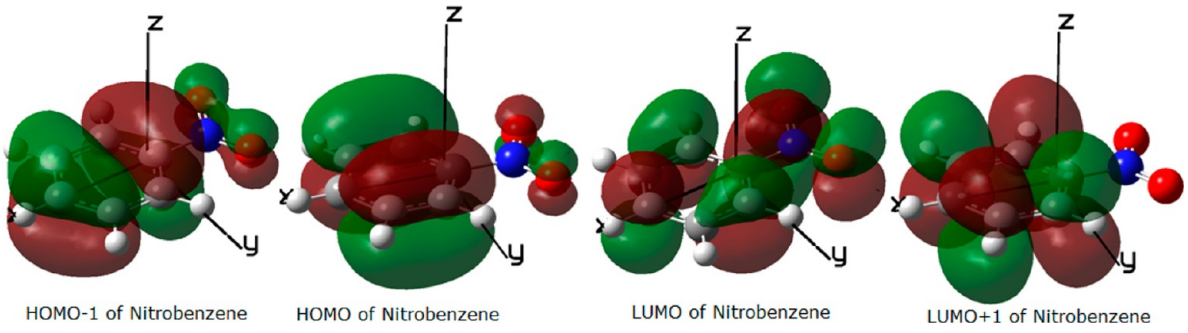

Figure 1. Electron-density surfaces for HOMO-1, HOMO, LUMO and LUMO+1 of nitrobenzene.

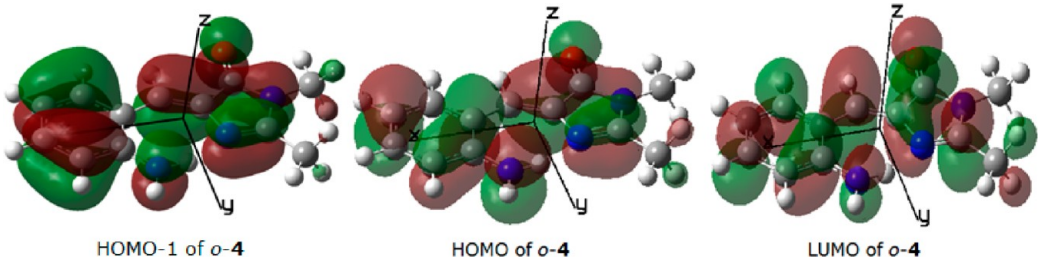

Figure 2. Electron density surfaces for HOMO-1, HOMO, and LUMO of *o*-**4**.

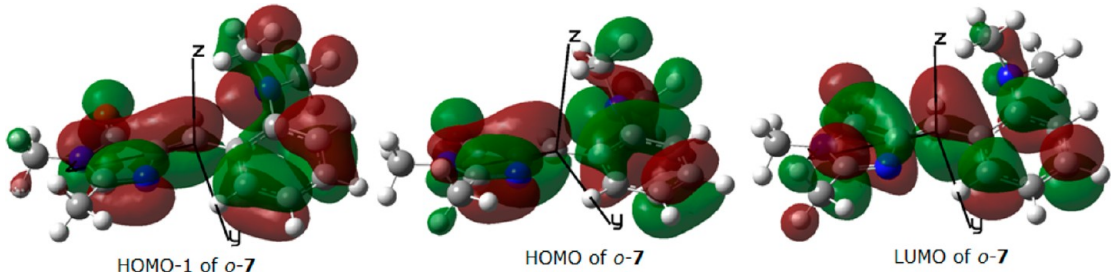

Figure 3. Electron-density surfaces for HOMO-1, HOMO, and LUMO of *o*-7.

oscillator strength (f) is 255 nm (f = 0.1963) at the B3LYP-TD/cc-PVTZ//B3LYP/6-31+G* level and 249 nm (f = 0.1902) at the B3LYP-TD/cc-PVDZ//B3LYP/6-31+G* level, both of which are in good agreement with the experimental results[9] (Table 2). The transition electric dipole moment calculated by TDDFT has been used to see if an electronic transition involves a charge transfer and to see the direction of electron transfer.[10] At the B3LYP-TD/cc-PVDZ//B3LYP/6-31+G* level, the transition electric dipole moment for the charge-transfer absorption of nitrobenzene at 249 nm is 1.248 au (3.2 D) along the x-axis, indicating that a substantial electron transfer has occurred from the benzene ring to the nitro group (Figure 1). This is consistent with the experimental results.[9]

We performed calculations on the electronic transitions of *o*-**4**, *o*-7, and *p*-7 at the B3LYP-TD/cc-PVDZ//B3LYP/6-31+G* level to understand whether their lowest energy electronic absorption bands involve a charge-transfer transition. The calculated lowest energy singlet electronic transition of *o*-**4** is contributed by 0.61[HOMO→LUMO]-0.18[HOMO-1→LUMO] and located at 415 nm with an oscillator strength (f) of 0.2894 and a transition electric dipole moment of −1.9 au (−4.87 D) along the x axis and −0.59 au (−1.51 D) along

dx.doi.org/10.1021/jo302050y | J. Org. Chem. 2013, 78, 301−310

the y axis, which is in good agreement with the experimental data (427 nm in cyclohexane with ε = 5167 $M^{-1}cm^{-1}$, which corresponds to oscillator strength (f) of 0.11 according to the equation[11] $f = 4.3 \times 10^{-9} \int \varepsilon d\nu = 4.3 \times 10^{-9} \times \varepsilon_{max} \times \Delta\nu_{1/2}$). The magnitude of this transition electric dipole moment is greater than those of the charge-transfer transitions of nitrobenzene and peridinin (3.2 D for nitrobenzene and 3.4 D for peridinin[10b]). Hence, we suggest that the lowest energy electronic absorption of *o*-**4** involves a charge-transfer transition. The negative sign of this transition electric dipole moment of *o*-**4** indicates that a substantial electron transfer has occurred from the imidazolone moiety to the aniline moiety during the excitation (Figure 2).

The calculated lowest energy singlet electronic transition of *o*-**7** is contributed by 0.58[HOMO→LUMO]-0.33[HOMO-1→LUMO] and located at 410 nm with an oscillator strength (f) of 0.2153 and a transition electric dipole moment of 1.7 au (4.36 D) along the x-axis, 0.05 au (0.13 D) along the y-axis, and −0.08 au (−0.21 D) along the z-axis, indicating that a substantial electron transfer has occurred from the imidazolone moiety to the aniline moiety during the excitation (Figure 3). According to the magnitude and sign of this transition electric dipole moment, we suggest that the lowest energy electronic absorption of *o*-**7** involves a charge-transfer transition. This result is in good agreement with the experimental data (395 nm in cyclohexane with ε = 7940 M^{-1} cm^{-1}, which corresponds to an oscillator strength (f) of 0.17).

The calculated lowest energy singlet electronic transition of *p*-**7** is contributed by 0.61[HOMO→LUMO] and located at 382 nm with an oscillator strength (f) of 0.9418 and a transition electric dipole moment of −3.4 au (−8.72 D) along the x-axis and 0.11 au (0.28 D) along the y-axis, indicating that a substantial electron transfer has occurred from the aniline moiety to the imidazolone moiety during the excitation (Figure 4). This is opposite to those of *o*-**4** and *o*-**7**, indicating that the orientation of aniline has a significant influence on the direction of electron transfer in the charge-transfer transition. According to the magnitude and sign of this transition electric dipole moment, we suggest that the lowest energy electronic absorption of *p*-**7** involves a charge-transfer transition. This result is in good agreement with the experimental data (405 nm in cyclohexane with ε = 23966 M^{-1} cm^{-1}, which corresponds to an oscillator strength (f) of 0.52).

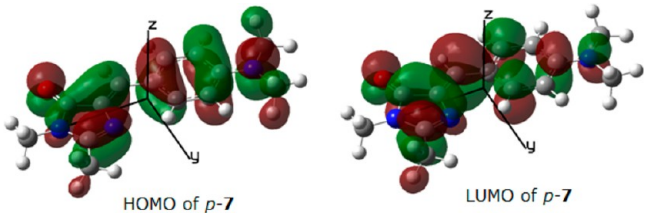

Figure 4. Electron-density surfaces for HOMO and LUMO of *p*-**7**.

The lowest energy electronic absorption of *p*-**7** is red-shifted in the polar solvents. This is likely because the charge-transfer excited-state is more polar than the ground-state and the dipole−dipole interactions with solvent molecules lower the energy of the excited state more than that of the ground state.[11] This red-shift trend is not found for the lowest energy electronic absorption of *o*-**4** and *o*-**7** in the polar solvents, even though they also involve a charge-transfer transition. This is likely because steric hindrance between the aniline and the imidazolone moieties plays a more important role. The lowest energy electronic absorption bands of *o*-**4** and *o*-**7** in water are significantly blue-shifted relative to those in other solvents, and this is likely attributed to the increasing twist angle between the aniline and the imidazolone moieties, which is caused by the strong solvation in water through intermolecular hydrogen bonding. In addition, the significant blue-shift for the lowest energy electronic absorption band of *o*-**7** relative to that of *o*-**4** is also attributed to the increasing twist angle between the aniline and the imidazolone moieties.

The *o*-**4** displays dual fluorescence in acetonitrile: one at 453 nm that is not sensitive to solvent polarity and is ascribed to radiation relaxation from the locally excited (LE)[12] state and the other at 524 nm that is sensitive to solvent polarity (Figure 5). The *p*-**4** is nonfluorescent, while the emissions at 536 nm of *o*-**7** and at 483 nm of *p*-**7** in acetonitrile are also sensitive to solvent polarity (Figures 6 and 7). According to the Lippert−Mataga equation[13] (eq 1), solvatochromic Stokes shifts ($\Delta\nu$) of the longest wavelength emission of *o*-**4**, *o*-**7**, and *p*-**7** were plotted as a function of the solvent polarity parameter Δf (Figure 8). These three Lippert−Mataga plots are linear, and their slopes ($\Delta\nu/\Delta f$) in combination with the radius of the cavity (a) can be used to calculate the dipole moment changes ($\Delta\mu$) from the ground states to the first singlet excited states of *o*-**4**, *o*-**7**, and *p*-**7**, which were calculated to be 10.8, 10.9, and 7.9 D, respectively, indicating that the first singlet excited-states of *o*-**4**, *o*-**7**, and *p*-**7** bear significant charge-transfer character. Hence, the longest wavelength emissions of *o*-**4**, *o*-**7** and *p*-**7** are ascribed to radiation relaxation from the twisted internal charge-transfer (TICT)[12] states. The first singlet excited state

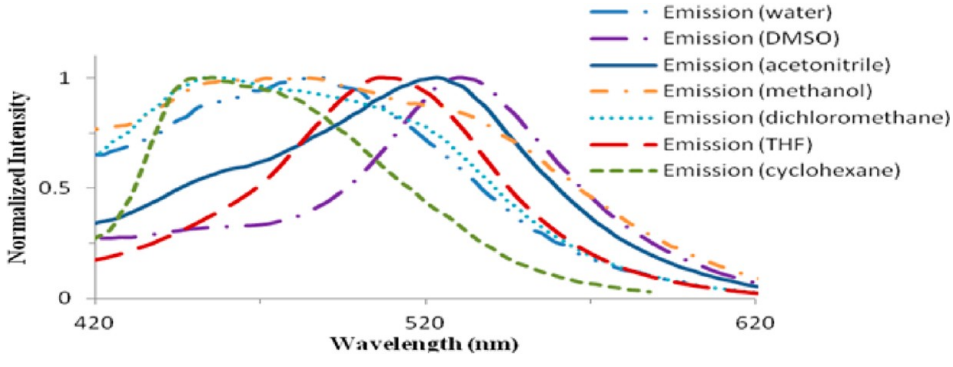

Figure 5. Emission spectra of *o*-**4** in various solvents.

dx.doi.org/10.1021/jo302050y | J. Org. Chem. 2013, 78, 301−310

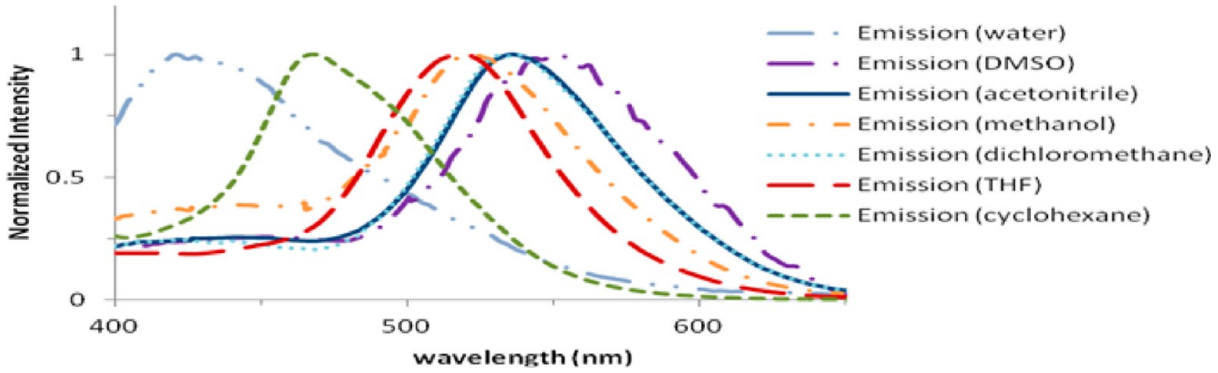

Figure 6. Emission spectra of *o*-7 in various solvents.

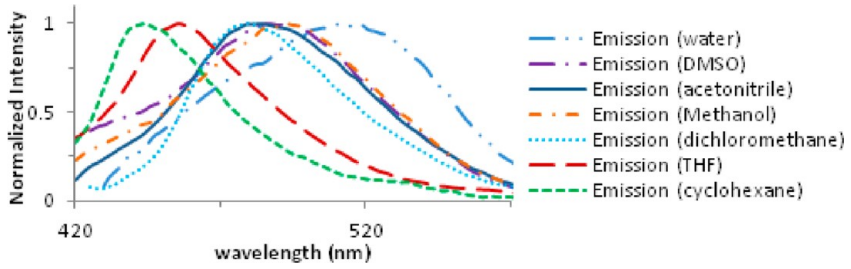

Figure 7. Emission spectra of *p*-7 in various solvents.

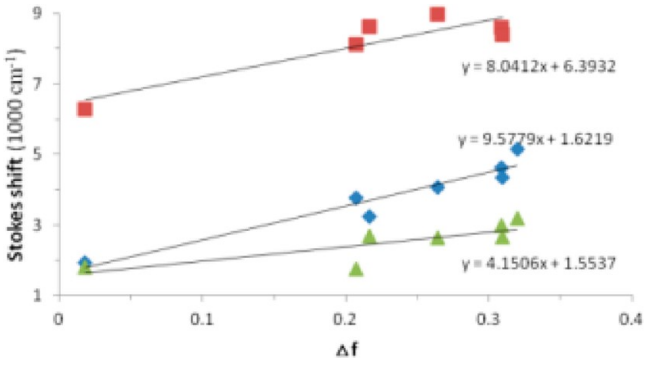

Figure 8. Lippert–Mataga plots of *o*-4 (blue dot), *o*-7 (red dot), and *p*-7 (green dot).

of *p*-7 shows less charge-transfer character than those of *o*-4 and *o*-7, indicating that a longer distance between electron-donor and electron-acceptor reduces charge-transfer degree. This is consistent with the Rehm–Weller equation.[14] In contrast to *o*-7 and *p*-7, the dual fluorescence of *o*-4 is found in less polar solvents of dichloromethane and cyclohexane and protic solvents of methanol and water. It is likely that the intramolecular hydrogen bonding through N–H···N or a series of protic solvent molecules makes the emission from the LE state comparable relative to that from the TICT state, where $\Delta f = [(\varepsilon - 1)/(2\varepsilon + 1)] - [(n^2 - 1)/(2n^2 + 1)]$ and a is the radius of the cavity in which the solute resides (a = 4.97, 5.32, 5.33 Å for *o*-4, *o*-7 and *p*-7 at B3LYP/6-31+G* level).

$$\Delta\nu = \nu_{abs} - \nu_{em} = [2/(4\pi\varepsilon_0 hc)][(\Delta\mu)^2/a^3](\Delta f) + \text{constant} \quad (1)$$

Application. Because the first-singlet excited-states of *o*-4 and *o*-7 carry significant charge-transfer character through the PCT mechanism, they have potential to become wavelength-ratiometric fluorescence sensors, which permit ratiometric measurements of fluorescence to be made and allow the determination of cation concentration independently of various parameters like sensor concentration and incident-light intensity.[15]

Absorption and fluorescence titrations of *o*-4 or *o*-7 with various cations of group I (Na^+, K^+), group II (Mg^{2+}, Ca^{2+}), and heavy metals (Pb^{2+}, Zn^{2+}, Ni^{2+}, Co^{2+}, Ag^+, Fe^{2+}, Fe^{3+}, Cu^{2+}, and Cr^{3+}) were performed in aqueous CH_3CN (6:4) at 25 °C. What we found was that both *o*-4 and *o*-7 can selectively recognize Cr^{3+}.

We synthesized the 1:3 Cr^{3+}/*o*-4 complex by mixing the concentrated *o*-4 with 0.33 equiv of concentrated $Cr(NO_3)_{3(aq)}$ in methanol for 30 min at room temperature until *o*-4 was completely consumed. We monitored this reaction by thin-layer chromatography (TLC). The emission maximum of the 1:3 Cr^{3+}/*o*-4 complex in aqueous CH_3CN (6:4) is at 450 nm, which is blue-shifted relative to that of *o*-4 (550 nm) (Figure 9). When the concentrated *o*-4 was treated with 1.0 equiv of concentrated $Cr(NO_3)_{3(aq)}$, the emission maximum of the product was blue-shifted from 550 to 400 and 380 nm. The dual emission maxima were assigned to the 1:2 and 1:1 Cr^{3+}/*o*-4 complexes. When *o*-4 was treated with 230 equiv of Cr^{3+}, its emission maximum at 380 nm increased but the one at 400 nm faded away. Hence, the product was supposed to be the 1:1 Cr^{3+}/*o*-4 complex. Similar phenomena were also found in the case of *o*-7.

To see if ethylenediamine competes with *o*-4 in the recognition of Cr^{3+}, the 1:3 Cr^{3+}/*o*-4 complex was titrated with excess ethylenediamine (Figure 10). During the fluorescence titration, the emission maximum was blue-shifted from the 1:3 Cr^{3+}/*o*-4 complex to the 1:1 Cr^{3+}/*o*-4 complex. This indicates that ethylenediamine ligand easily displaces the first two bidentate ligands of *o*-4 in the 1:3 Cr^{3+}/*o*-4 complex but it does not displace the last bidentate ligand of *o*-4. This implies that the binding affinity between Cr^{3+} and *o*-4 is much

dx.doi.org/10.1021/jo302050y | J. Org. Chem. 2013, 78, 301–310

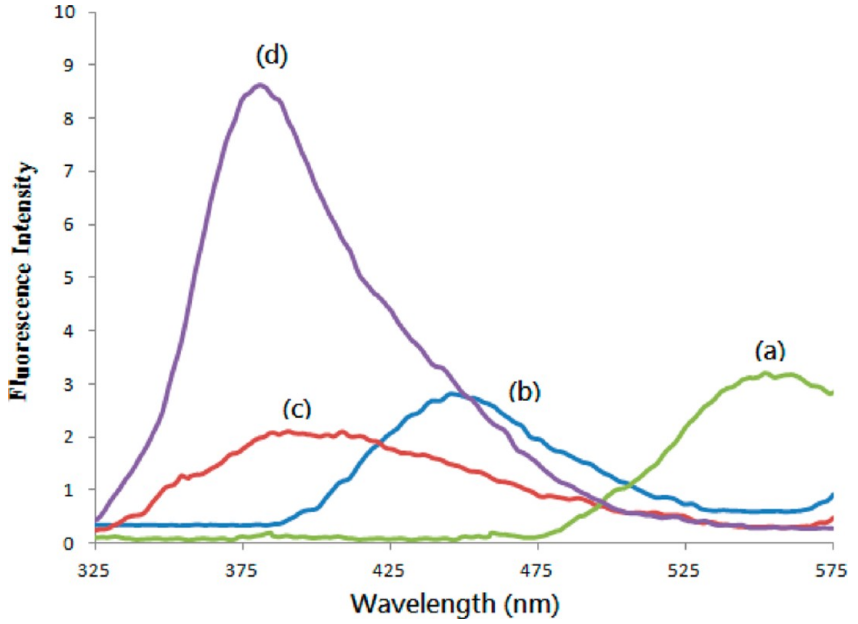

Figure 9. Emission spectra (λ_{ex} = 300 nm) in aqueous CH_3CN (6:4) for the products produced by mixing concentrated *o*-**4** with (a) 0, (b) 0.33, (c) 1.0, and (d) 230 equivalent of concentrated $Cr(NO_3)_{3(aq)}$ in methanol.

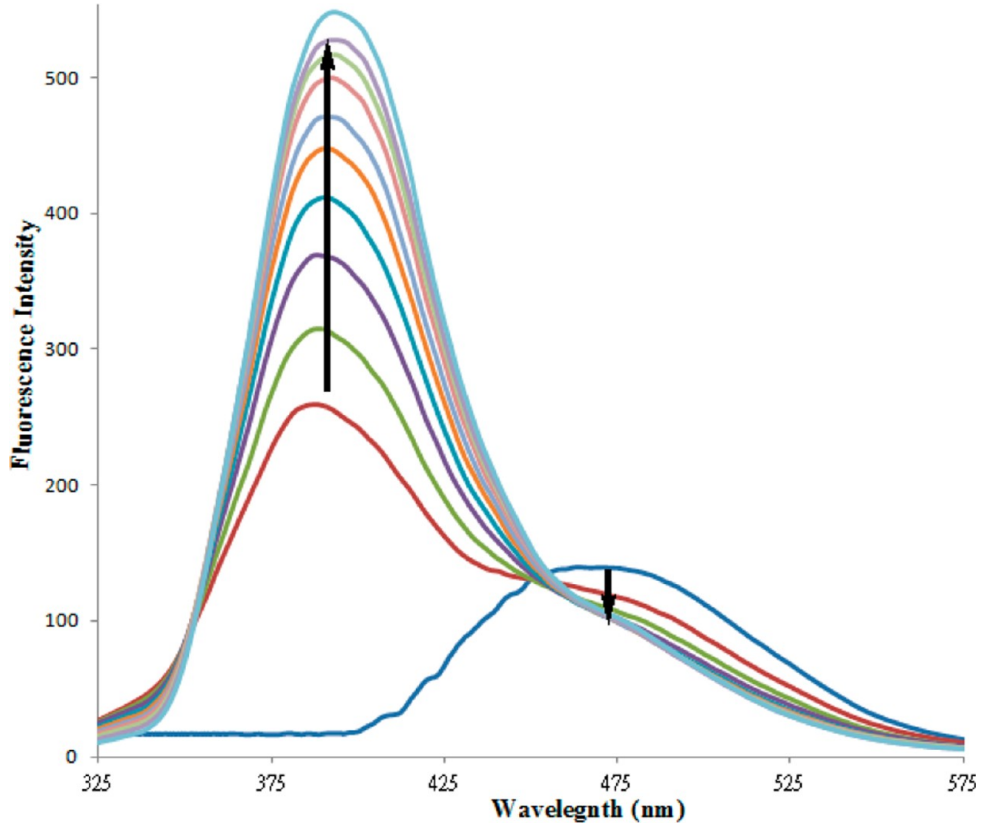

Figure 10. Fluorescence titration (λ_{ex} = 300 nm) of the 1:3 Cr^{3+}/*o*-**4** complex (1×10^{-4} M) with 0, 200, 400, 600, 800, 1000, 1200, 1400, 1600, 1800, and 2000 equiv of ethylenediamine in CH_3CN.

stronger than that between Cr^{3+} and ethylenediamine. The reason why the first two bidentate ligands of *o*-**4** in the 1:3 Cr^{3+}/*o*-**4** complex were easily displaced by ethylenediamine is likely because the bulky *o*-**4** causes significant steric tension in the 1:3 Cr^{3+}/*o*-**4** complex. Thus, we used the 1:1 Cr^{3+}/*o*-**4** (or *o*-**7**) complex as the final product in the recognition of Cr^{3+} with *o*-**4** or *o*-**7** and made sure that [*o*-**4**] or [*o*-**7**] was less than [Cr^{3+}].

In the UV−vis titration, upon addition of Cr^{3+}, the absorbance at 396 nm of *o*-**7** decreases gradually while the absorbance at 350 nm increases simultaneously, indicating that Cr^{3+} chelation reduces the resonance contribution from the

dx.doi.org/10.1021/jo302050y | *J. Org. Chem.* 2013, 78, 301−310

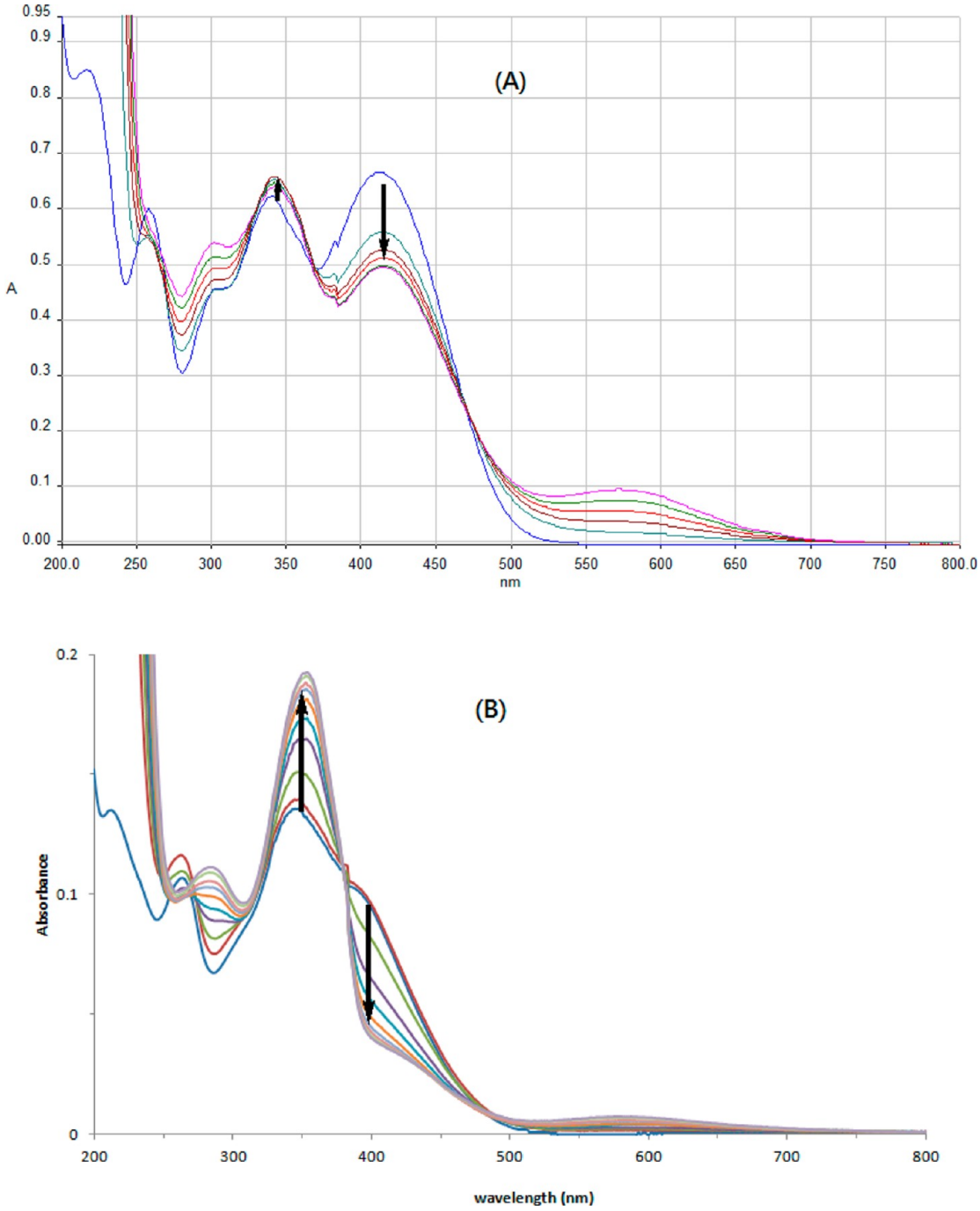

Figure 11. UV−vis titration of (A) *o*-**4** (1×10^{-4} M) with 0, 25.6, 51.2, 76.8, 102, and 128×10^{-4} M of $Cr(NO_3)_{3(aq)}$ and (B) *o*-**7** (1.8×10^{-5} M) with 0, 6.7, 13, 20, 27, 33, 40, 47, 53, and 60×10^{-5} M of $Cr(NO_3)_{3(aq)}$ in aqueous CH_3CN (6:4).

lone pair of electrons on N (Figure 11). Similar phenomena also occur in the UV−vis titration of *o*-**4**. There are isosbestic points that appear in the UV−vis titrations of *o*-**4** and *o*-**7** with Cr^{3+}, indicating that only one complex was formed in each titration system. According to Figure 9, we suggest that the only formed complex would be the 1:1 Cr^{3+}/*o*-**4** or Cr^{3+}/*o*-**7** complex.

For the fluorescence titration of *o*-**7** with Cr^{3+}, the emission at 545 nm decreases while a new emission at 422 nm increases with 6.7-fold fluorescence enhancement for 33.3 equiv of Cr^{3+} (Figure 12). The blue-shift in the emission spectrum is due to the diminishment of PCT, which is caused by the bidentate chelation of Cr^{3+} with *o*-**7**. The fluorescence intensity ratio ($F_{422\ nm}/F_{545\ nm}$) increases with the concentration of Cr^{3+}, and 33.3 equiv of Cr^{3+} is required to reach its saturation. According to Tsien's method,[16] the dissociation constant (K_d) of the 1:1 Cr^{3+}/*o*-**7** complex was estimated to be 94 μM. For the fluorescence titration of *o*-**4** with Cr^{3+}, the emission at 550 nm decreases while a new emission at 380 nm increases with 3.7-fold fluorescence enhancement for 230 equiv of Cr^{3+} (Figure 12). The fluorescence intensity ratio ($F_{380\ nm}/F_{550\ nm}$) of *o*-**4** increases with the concentration of Cr^{3+} until its saturation is reached at 230 equiv of Cr^{3+}. The dissociation constant (K_d) of the 1:1 Cr^{3+}/*o*-**4** complex was estimated to be 1.4 mM, which is around 10 times bigger than that of the 1:1 Cr^{3+}/*o*-**7** complex.

dx.doi.org/10.1021/jo302050y | *J. Org. Chem.* 2013, 78, 301−310

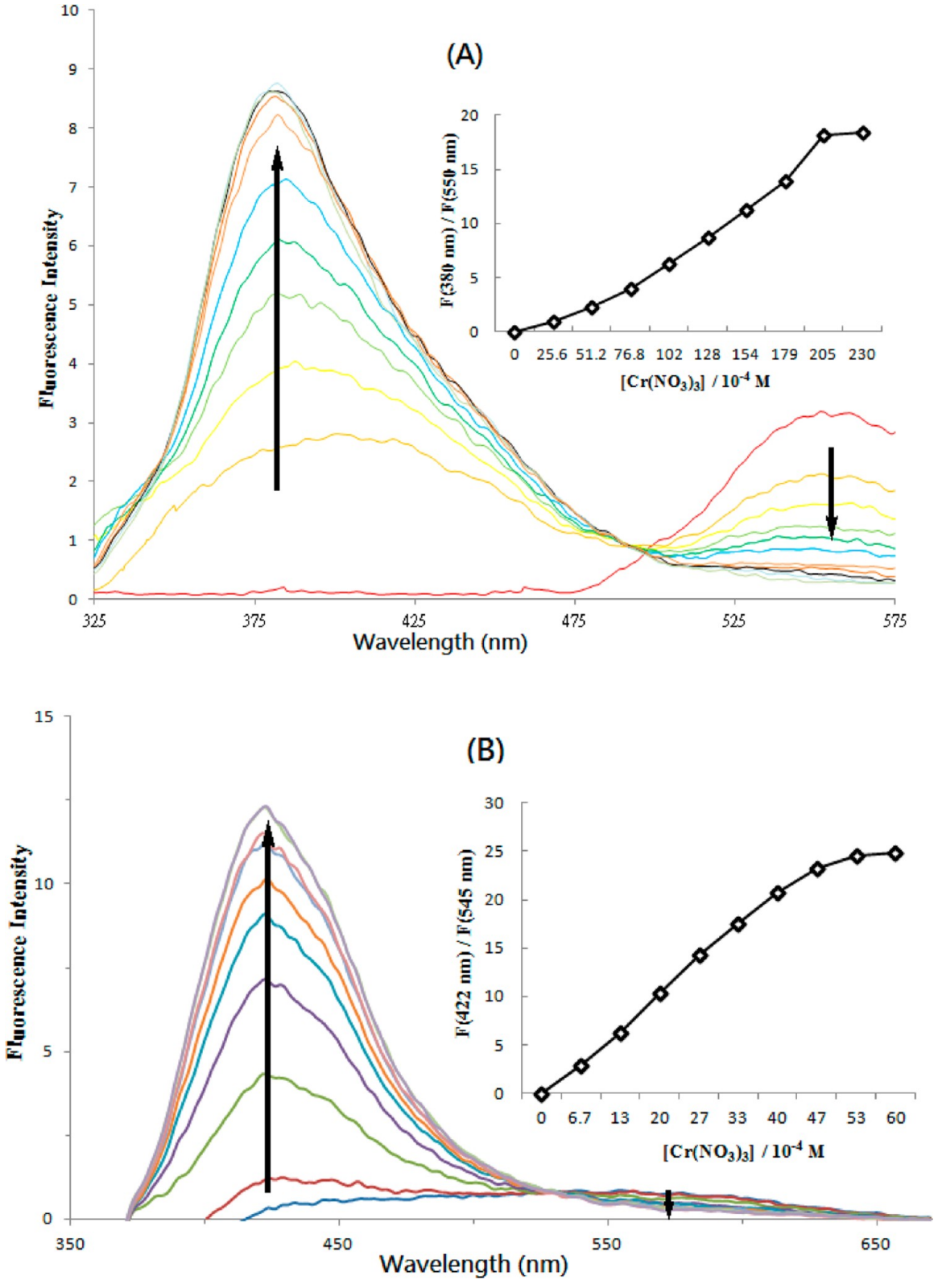

Figure 12. Fluorescence titration (λ_{ex} = 300 nm) of (A) *o*-**4** (1×10^{-4} M) with 0, 25.6, 51.2, 76.8, 102, 128, 154, 179, 205, and 230×10^{-4} M of $Cr(NO_3)_{3(aq)}$ and (B) *o*-**7** (1.8×10^{-5} M) with 0, 6.7, 13, 20, 27, 33, 40, 47, 53, and 60×10^{-5} M of $Cr(NO_3)_{3(aq)}$ in aqueous CH_3CN (6:4).

CONCLUSION

In the preparation of *o*-**4**, the *o*-acetamido, *o*-benzamido, and *o*-tosylamido groups fail to serve as protecting groups for the *o*-amino group. Not only do they get involved in the intramolecular cyclization, but the acetyl, benzoyl, and tosyl groups are also removed during the cyclization. The *o*-nitro protecting group is the only choice to synthesize the *o*-amino GFPSCs.

The lowest energy electronic absorption of *p*-**7** is red-shifted in the polar solvents, while this red-shift trend is not found for

dx.doi.org/10.1021/jo302050y | J. Org. Chem. 2013, 78, 301−310

the lowest energy electronic absorption of *o*-**4** and *o*-**7** in the polar solvents because the steric hindrance between the aniline and the imidazolone moieties play a more important role for the latter. Because of the increasing twist angle between the aniline and the imidazolone moieties by strong solvation in water, the lowest energy electronic absorption bands of *o*-**4** and *o*-**7** in water are significantly blue-shifted relative to those in other solvents. The first singlet excited states of *o*-**4**, *o*-**7**, and *p*-**7** carry significant charge-transfer character through the mechanism of PCT.

Both *o*-**4** and *o*-**7** can serve as wavelength-ratiometric fluorescence sensors that selectively recognize Cr^{3+} and can be used in aqueous medium.

EXPERIMENTAL SECTION

Materials and Methods. The *o*-**1a**,[17a] *o*-**1b**,[17b] *o*-**1c**,[17c] *o*-**2d**,[17d] *p*-**4**,[17e] and *p*-**7**[17f] are known and prepared according to the literature methods. High-resolution mass (HRMS) measurements were obtained with magnetic-electric sector mass analyzer.

1,2-Dimethyl-4-(2-nitrobenzylidene)-1*H*-imidazol-5(4*H*)-one (*o*-3d). To *o*-**2d** (3.48 g, 15 mmol) in 45 mL of THF was slowly added 40 wt % of methylamine (1.164g, 15 mmol). The mixture was stirred in a nitrogen atmosphere at room temperature for ∼20 min until the reaction was complete. The solution was concentrated by a rotary evaporator, and pyridine (7.5 mL) was added to the residue. The mixture was stirred under a nitrogen atmosphere under reflux for 5 h. After reaction, the solution was cooled, and some ice was added to the solution. The solution was stirred until most of the solid precipitated. The crude product was purified by column chromatography with hexane/ethyl acetate (1:1) as a mobile phase to obtain *o*-**3d**, and the yield was 55%: ^{1}H NMR ($CDCl_3$, 300 MHz) 2.37 (s, 3H, CH_3), 3.20 (s, 3H, CH_3), 7.48 (t, 1H, PhH), 7.50 (s, 1H, CH), 7.66 (t, 1H, PhH), 8.00 (d, 1H, PhH), 8.46 (d, 1H, PhH); ^{13}C NMR ($CDCl_3$, 75 MHz) 15.7, 26.7, 121.1, 124.6, 128.7, 129.7, 132.9, 133.6, 141.0, 149.2, 165.3, 169.9; HRMS (EI) *m*/*z* calcd for 245.08, $C_{12}H_{11}N_3O_3$ found 245.0799.;

***cis*-4-(2-Aminobenzylidene)-1,2-dimethyl-1*H*-imidazol-5(4*H*)-one (*o*-4).** To *o*-**3d** (1.9 g, 7.75 mmol) in 25 mL of MeOH was added 380 mg of 5% Pd/C. The mixture was stirred under a hydrogen atmosphere (1 atm) at room temperature for 2−3 h until the reaction was complete. After filtration, the filtrate was concentrated by a rotary evaporator. The crude product was purified by column chromatography with hexane/ethyl acetate (1:1) as mobile phase to obtain *o*-**4**, and the yield was 70%: ^{1}H NMR ($CDCl_3$, 300 MHz) δ 2.32 (s, 3H, CH_3), 3.18 (s, 3H, CH_3), 6.25 (s. 1H, NH), 6.62−6.66 (m, 2H, PhH), 7.15 (t, J = 7.3 Hz, 1H, PhH), 7.21 (s, 1H, CH), 7.49 (d, J = 7.9 Hz, 1H, PhH); ^{13}C NMR ($CDCl_3$, 75 MHz) δ 15.5, 26.7, 116.8, 117.2, 117.8, 128.9, 132.6, 133.9, 136.1, 148.2, 158.1, 169.9; HRMS (EI, M^+) *m*/*z* calcd for $C_{12}H_{13}N_3O$ 215.1059, found 215.1055.

3-Acetamido-2-quinolinone (5). To 0.5 mL of acetic anhydride was added *N*-acetylglycine (128 mg, 1.1 mmol). The mixture was stirred under a nitrogen atmosphere at 120 °C for 10 min. The aldehyde substrate (*o*-**1a**, *o*-**1b**, or *o*-**1c**, 1 mmol) and sodium acetate (123 mg, 1.5 mmol) were added into the solution and the resulting solution stirred under reflux for 18 h. The solution was extracted with ethyl acetate, and the extracted solution was dried with anhydrous sodium sulfate and concentrated by a rotary evaporator. The crude product was purified by column chromatography with hexane/ethyl acetate (1:1) as a mobile phase to get **5**, and yields were 78, 60, or 66%, respectively: ^{1}H NMR ($CDCl_3$, 300 MHz) δ 2.29 (s, 3H, CH_3), 7.23−7.32 (m, 2H, PhH × 2), 7.44 (t, 1H, PhH), 7.61 (d, 1H, PhH), 8.46 (bs, 1H, NH), 8.82 (s, 1H, CH), 11.31 (s(broad), 1H, NH); ^{13}C NMR ($CDCl_3$, 75 MHz) δ 24.8, 115.3, 120.7, 122.0, 123.5, 127.8, 127.9, 128.6, 133.5, 158.7,169.2; HRMS (FAB, M^+) *m*/*z* calcd for $C_{11}H_{10}N_2O_2$ 202.0742, found 202.0742.

2(1*H*)-Quinolinone (6). To 0.5 mL of acetic anhydride were added 2-acetylamidobenzaldehyde (*o*-**1a**) (163 mg, 1 mmol) and sodium acetate (123 mg, 1.5 mmol). The mixture was stirred under a nitrogen atmosphere under reflux for 18 h. The solution was extracted with ethyl acetate, and the extracted solution was dried with anhydrous sodium sulfate and concentrated by a rotary evaporator. The crude product was purified by column chromatography with hexane/ethyl acetate (3:1) as a mobile phase to obtain **6**, and the yield was 76%: ^{1}H NMR ($CDCl_3$, 300 MHz) δ 6.74 (d, 1H, CH), 7.22 (t, 1H, PhH), 7.43−7.58 (m, 3H, PhH × 3), 7.82 (d, 1H, CH), 12.51 (s(broad), 1H, NH); ^{13}C NMR ($CDCl_3$, 75 MHz) δ 116.2, 119.9, 121.3, 122.7, 127.8, 130.7, 138.4, 141.1, 164.6. The data obtained for the products are in agreement with those reported in the literature.[17g]

***cis*-4-(2-(Dimethylamino)benzylidene)-1,2-dimethyl-1*H*-imidazol-5(4*H*)-one (*o*-7).** To *o*-**4** (215 mg, 1 mmol) and sodium carbonate (212 mg, 2 mmol) in 3 mL of dried THF was slowly added iodomethane (292 mg, 2 mmol). The mixture was stirred under a nitrogen atmosphere at room temperature until the reaction was complete. The solution was extracted with ethyl acetate, and the extracted solution was dried with anhydrous sodium sulfate and concentrated by a rotary evaporator. The crude product was purified by column chromatography with hexane/ethyl acetate (1:1) as the mobile phase to obtain *o*-**7**, and the yield was 55%: ^{1}H NMR ($CDCl_3$, 300 MHz) δ 2.38 (s, 3H, CH_3), 2.78 (s, 6H, CH_3), 3.20 (s, 3H, CH_3), 7.01−7.07 (m, 2H, PhH), 7.30 (t, J = 7.4 Hz, 1H, PhH), 7.56 (s, 1H, CH), 8.44 (d, J = 7.4 Hz, 1H, PhH); ^{13}C NMR ($CDCl_3$, 75 MHz) δ 15.6, 26.6, 45.2, 117.9, 122.1, 125.5, 127.1, 130.7, 133.1, 137.5, 155.1, 161.5, 170.8; HRMS (EI, M^+) *m*/*z* calcs for $C_{14}H_{17}N_3O$ 243.1372, found 243.1367.

ASSOCIATED CONTENT

Supporting Information

Energy and redundant internal coordinates of *o*-**4**, *o*-**7**, and *p*-**7**, ^{1}H and ^{13}C NMR spectra of *o*-**3d**, *o*-**4**, **5**, **6**, *o*-**7**, and *p*-**7**, and electronic absorption spectra of *o*-**4**, *o*-**7**, and *p*-**7** in various solvents. This material is available free of charge via the Internet at http://pubs.acs.org.

AUTHOR INFORMATION

Corresponding Author

*E-mail: kssung@mail.ncku.edu.tw.

Notes

The authors declare no competing financial interest.

ACKNOWLEDGMENTS

We thank National Science Council of Taiwan for financial support (NSC101-2113-M-006-001-MY3).

REFERENCES

(1) (a) Pakhomov, A. A.; Martynov, V. I. *Chem. Biol.* **2008**, *15*, 755. (b) Shaner, N. C.; Patterson, G. H.; Davidson, M. W. *J. Cell Sci.* **2007**, *120*, 4247.

(2) (a) Hsieh, C. C.; Chou, P. T.; Shih, C.-W.; Chuang, W.-T.; Chung, M.-W.; Lee, J.; Joo, T. *J. Am. Chem. Soc.* **2011**, *133*, 2932. (b) Dong, J.; Solntsev, K. M.; Poizat, O.; Tolbert, L. M. *J. Am. Chem. Soc.* **2007**, *129*, 10084. (c) Chen, K.-Y.; Cheng, Y.-M.; Lai, C.-H.; Hsu, C.-C.; Ho, M.-L.; Lee, G.-H.; Chou, P.-T. *J. Am. Chem. Soc.* **2007**, *129*, 4534.

(3) Yang, J.-S.; Huang, G.-J.; Liu, Y.-H.; Peng, S.-M. *Chem. Commun.* **2008**, 1344.

(4) (a) Arakawa, H. *J. Biol. Chem.* **2000**, *275*, 10150. (b) Anderson, R.; Chromium, R. A. *Trace Elements in Human and Animal Nutrition*; Academic Press: New York, 1987. (c) Vincent, J. B. *Nutr. Rev.* **2000**, *58*, 67. (d) Eastmond, D. A.; MacGregor, J. T.; Slesinski, R. S. *Crit. Rev. Toxicol.* **2008**, *38*, 173.

(5) (a) Han, Y.; You, Y.; Lee, Y.-M.; Nam, W. *Adv. Mater.* **2012**, *24*, 2748. (b) Zhou, Z.; Yu, M.; Yang, H.; Huang, K.; Li, F.; Yi, T.; Huang, C. *Chem. Commun.* **2008**, 3387. (c) Panda, S.; Pati, P. B.; Zade, S. S. *Chem. Commun.* **2011**, *47*, 4174. (d) Wang, D.; Shiraishi, Y.; Hirai, T. *Tetrahedron Lett.* **2010**, *51*, 2545. (e) Wu, H.; Zhou, P.; Wang, J.; Zhao, L.; Duan, C. *New J. Chem.* **2009**, *33*, 653. (f) Weerasinghe, A. J.; Schmiesing, C.; Sinn, E. *Tetrahedron Lett.* **2009**, *50*, 6407. (g) Huang, K.; Yang, H.; Zhou, Z.; Yu, M.; Li, F.; Gao, X.; Yi, T.; Huang, C. *Org. Lett.* **2008**, *10*, 2557. (h) Mao, J.; Wang, L.; Dou, W.; Tang, X.; Yan, Y.; Liu, W. *Org. Lett.* **2007**, *9*, 4567. (i) Sarkar, M.; Bandip, S.; Samanta, A. *Tetrahedron Lett.* **2006**, *47*, 7575.

(6) Frisch, M. J.; Trucks, G. W.; Schlegel, H. B.; Scuseria, G. E.; Robb, M. A.; Cheeseman, J. R.; Montgomery, J. A., Jr.; Vreven, T.; Kudin, K. N.; Burant, J. C.; Millam, J. M.; Iyengar, S. S.; Tomasi, J.; Barone, V.; Mennucci, B.; Cossi, M.; Scalmani, G.; Rega, N.; Petersson, G. A.; Nakatsuji, H.; Hada, M.; Ehara, M.; Toyota, K.; Fukuda, R.; Hasegawa, J.; Ishida, M.; Nakajima, T.; Honda, Y.; Kitao, O.; Nakai, H.; Klene, M.; Li, X.; Knox, J. E.; Hratchian, H. P.; Cross, J. B.; Adamo, C.; Jaramillo, J.; Gomperts, R.; Stratmann, R. E.; Yazyev, O.; Austin, A. J.; Cammi, R.; Pomelli, C.; Ochterski, J. W.; Ayala, P. Y.; Morokuma, K.; Voth, G. A.; Salvador, P.; Dannenberg, J. J.; Zakrzewski, V. G.; Dapprich, S.; Daniels, A. D.; Strain, M. C.; Farkas, O.; Malick, D. K.; Rabuck, A. D.; Raghavachari, K.; Foresman, J. B.; Ortiz, J. V.; Cui, Q.; Baboul, A. G.; Clifford, S.; Cioslowski, J.; Stefanov, B. B.; Liu, G.; Liashenko, A.; Piskorz, P.; Komaromi, I.; Martin, R. L.; Fox, D. J.; Keith, T.; Al-Laham, M. A.; Peng, C. Y.; Nanayakkara, A.; Challacombe, M.; Gill, P. M. W.; Johnson, B.; Chen, W.; Wong, M. W.; Gonzalez, C.; Pople, J. A. *Gaussian 03, Revision A.1*; Gaussian, Inc.: Pittsburgh, PA, 2003.

(7) Juarez-Gordiano, C.; Hernandez-Campos, A.; Castillo, R. *Synth. Commun.* **2002**, *32*, 2959−2963.

(8) Gucky, T.; Slouka, J.; Wiedermannova, L. *Heterocycl. Commun.* **2003**, *9*, 437.

(9) Zhu, X.-M.; Zhang, S.-Q.; Zheng, X.; Phillips, D. L. *J. Phys. Chem. A* **2005**, *109*, 3086.

(10) (a) Tiwary, A. S.; Sengupta, P. S.; Mukherjee, A. K. *Chem. Phys. Lett.* **2007**, *433*, 427. (b) Vaswani, H. M.; Hsu, C.-P.; Head-Gordon, M.; Fleming, G. R. *J. Phys. Chem. B* **2003**, *107*, 7940.

(11) Turro, N. J.; Ramamurthy, V.; Scaiano, J. C. *Modern Molecular Photochemistry of. Organic Molecules*; University Science Publishers: New York, 2010.

(12) Grabowski, Z. R.; Rotkiewicz, K. *Chem. Rev.* **2003**, *103*, 3899.

(13) Zucchero, A. J.; Tolosa, J.; Tolbert, L. M.; Bunz, U. H. F. *Chem.—Eur. J.* **2009**, *15*, 13075.

(14) Rehm, D.; Weller, A. *Isr. J. Chem.* **1970**, *8*, 259.

(15) Leray, I.; Lefevre, J.-P.; Delouis, J.-F.; Delaire, J.; Valeur, B. *Chem.—Eur. J.* **2001**, *7*, 4590.

(16) Tsien, R. Y. *Methods Cell Biol.* **1989**, *30*, 127.

(17) (a) Schwarz, M. K.; Quattropani, A.; Dorbais, J.; Covini, D.; Pittet, P. A.; Colovray, V.; Thomas, R. J.; Coxhead, R.; Halazy, S.; Scheer, A.; Missotten, M.; Ayala, G.; Bradshaw, C.; De Raemy-Schenk, A. M.; Nichols, A.; Cirillo, R.; Tos, E. G.; Giachetti, C.; Golzio, L.; Marinelli, P.; Church, D. J.; Barberis, C.; Chollet, A. *J. Med. Chem.* **2005**, *48*, 7882. (b) Lin, W. W.; Syu, S. E.; Lee, Y. T.; Jang, Y. J. *Org. Lett.* **2011**, *13*, 2970. (c) Liu, F.; Anstiss, C. *Tetrahedron* **2010**, *66*, 5486. (d) Mazurov, A. A.; Andronati, S. A.; Antonenko, V. V. *Chem. Heterocycl. Compd.* **1985**, *21*, 514. (e) Yang, J. S.; Huang, G. J.; Liu, Y. H.; Peng, S. M. *Chem Commun* **2008**, 1344. (f) Lee, J. S.; Badridge, A.; Peng, S. H.; Yang, S. Q.; Kim, Y. K.; Tolbert, L. M.; Chang, Y. T. *ACS Comb. Sci.* **2011**, *13*, 32. (g) Kobayashi, Y.; Kamisaki, H.; Takeda, H.; Yasui, Y.; Yanada, R.; Takemoto, Y. *Tetrahedron* **2007**, *63*, 2978.